Original Research

Manipulating Histone Acetylation Leads to Antitumor Effects in Hemangiosarcoma Cells

Tamami Suzuki [1], Keisuke Aoshima [1]*, Jumpei Yamazaki [2], Atsushi Kobayashi [1], Takashi Kimura [1]

[1] *Laboratory of Comparative Pathology, Department of Clinical Sciences, Faculty of Veterinary Medicine, Hokkaido University, Sapporo, Hokkaido, 060-0818, Japan*

[2] *Translational Research Unit, Veterinary Teaching Hospital, Faculty of Veterinary Medicine, Hokkaido University, Sapporo, Hokkaido, 060-0818, Japan*

Running title: Histone Acetylation in Hemangiosarcoma

* Corresponding author. Tel.: +81 11 7065193.

E-mail address: k-aoshima@vetmed.hokudai.ac.jp (Keisuke Aoshima).

Acknowledgements

We would like to extend our sincerest gratitude to Dr. Hiroki Sakai, Gifu University, for providing canine hemangiosarcoma cell lines. We also acknowledge the efforts of Drs. Mitsuyoshi Takiguchi, Shintaro Kobayashi, and Hironobu Yasui, Faculty of Veterinary Medicine, Hokkaido University for giving useful pieces of advice and constructive discussion. We are grateful to all the members of the Laboratory of Comparative Pathology, Faculty of Veterinary Medicine, Hokkaido University for their helpful discussions,

encouragement, and support. This research was supported by KAKENHI Grant-in-Aid for Young Scientists (KA, Number 20K15654) provided by Japan Society for the Promotion of Science. We thank H. Nikki March, PhD, from Edanz (https://jp.edanz.com/ac) for editing a draft of this manuscript.

Conflict of interest statement

The authors declare that there is no conflict of interest in this study.

Ethics statement

The owners were thoroughly informed about the research aims and protocols, and a written consent form was obtained prior to the investigation. All mouse experiments were performed under the guidelines of Hokkaido University (protocol number: 20-0083), which follows the ARRIVE guidelines.

Preprint

The preprint of this manuscript was uploaded on bioRxiv.

https://www.biorxiv.org/content/10.1101/2021.12.10.472173v2

Data availability

The datasets generated and/or analyzed during the current study are available from the corresponding author on reasonable request.

RNA-seq data was uploaded on Gene Expression Omnibus (GEO accession GSE200106). This will be published when this manuscript is accepted. To review GEO accession GSE200106, please visit https://www.ncbi.nlm.nih.gov/geo/query/acc.cgi?acc=GSE200106.

Original Research

Title

Manipulating Histone Acetylation Leads to Antitumor Effects in Hemangiosarcoma Cells

Word count: 4000 words

Number of figures: 6

Number of Tables: 0

Abstract

Canine hemangiosarcoma (HSA) is a malignant tumor derived from endothelial cells. No effective treatment has yet been developed because of the lack of understanding of its pathogenesis. Histone acetylation, an epigenetic modification, is highly associated with cancer pathogenesis. Manipulating histone acetylation by histone deacetylase inhibitors (HDACi) or bromodomain and extraterminal domain inhibitors (BETi) is one approach to treat various cancers. However, the role of histone acetylation in HSA remains unknown. This study aimed to investigate how histone acetylation functions in HSA pathogenesis using two HDACi, suberanilohydroxamic acid (SAHA) and valproic acid (VPA), and one BETi, JQ1, *in vitro* and *in vivo*. Histone acetylation levels were high in cell lines and heterogeneous in clinical cases. SAHA and JQ1 induced apoptosis in HSA cell lines. HSA cell lines treated with SAHA and VPA upregulated inflammatory-related genes and attracted macrophage cell line RAW264 cells, which suggests that SAHA and VPA can affect immune responses. JQ1 stimulated autophagy and inhibited the cell cycle in HSA cell lines. Finally, we demonstrated that JQ1 suppressed HSA tumor cell proliferation *in vivo* although SAHA and VPA did not affect tumor growth. These results suggest that BETi can be alternative drugs for HSA treatment. Although further research is required, our study indicated that dysregulation of histone acetylation is likely to be involved in HSA malignancy.

Keywords

BETi; HDACi; hemangiosarcoma; histone acetylation

1. INTRODUCTION

Canine hemangiosarcoma (HSA) is a malignant tumor derived from endothelial cells. It is characterized by invasive growth and high metastatic rates, which causes high mortality to patients.[1] Surgery and chemotherapy are conventional therapies for HSA, but the efficacy of these treatments was limited.[2] Angiosarcoma (AS), a counterpart of HSA in humans, has similar clinicopathological features to HSA.[3,4] Somatic mutations in *PIK3CA*, *TP53* or *RASA1* were identified in both HSA and AS,[5] but little is known about how these mutations relate to HSA and AS pathogenesis.

Epigenetics such as DNA methylation and histone modifications regulates transcription, and it is involved in various biological processes such as embryonic development, metabolism, and diseases including cancer.[6–8] Acetylated histone can promote transcription by binding to bromodomain and extraterminal (BET) proteins and loosening the chromatin structure by neutralizing the electric charges.[9,10] In recent years, a growing number of reports have highlighted that altered histone acetylation is involved in cancer pathogenesis.[11,12] Histone deacetylase inhibitors (HDACi) and BET inhibitors (BETi) have been used to investigate the function of histone acetylation and their treatment efficacy. HDACi increased histone acetylation levels by inhibiting histone deacetylase function.[13] BETi binds to the functional domain of BET proteins through which BET proteins cannot recognize acetylated histones.[14] Suberanilohydroxamic acid (SAHA) and valproic acid (VPA) are HDACis that have been reported to induce apoptosis *in vitro* and suppress tumor proliferation *in vivo* in human cancers.[15–18] SAHA and VPA can also improve tumor immunity, and combination therapies with immune checkpoint inhibitors or chemotherapeutics enhance their efficacy in human cancers.[19–21] BETi has also been broadly investigated as cancer drugs, including JQ1, which causes apoptosis, cell cycle arrest, and autophagy *in vitro*, and impede tumor growth *in vivo*.[22–24] Regarding epigenetics in HSA,

KDM2B—a histone demethylase—has recently been found to promote tumor viability.[25] However, the role of histone acetylation in HSA remains unknown.

Immune cells in tumor tissues play important roles in tumor progression as major components of the tumor microenvironment. Some immune cells such as natural killer cells, cytotoxic T cells, and M1-polarized macrophages attack tumor cells and inhibit tumor growth, whereas other cells such as regulatory T cells and M2-polarized macrophages promote tumor growth by secreting protumor cytokines or suppressing immune responses against tumor cells.[26,27] Given that tumor cells dynamically interact with immune cells in tumor tissues, investigating tumor pathogenesis in immunocompetent environments is crucial to develop new therapeutics such as immunotherapy and metabolic therapy.[28–30] A mouse-derived AS cell line ISOS-1, which is transplantable in BALB/c mice, has recently been revealed to have similar morphological and molecular characteristics to canine HSA cell lines.[31,32] Identifying pathological similarities between canine HSA cell-derived tumors and murine AS cell-derived tumors in mice would be beneficial to find novel therapeutics involving the host immune system by promoting syngeneic mouse model studies in HSA.

In this study, we aimed to investigate the role of histone acetylation and the effects of HDACi and BETi on HSA. We used canine HSA cell lines and ISOS-1, a mouse AS cell line, to explore whether they have similar responses to HDACi and BETi treatments and to research their effects in both immunodeficient and immunocompetent environments.

2. MATERIALS AND METHODS

Full materials and methods are available in the supporting information.

2.1 Histopathology and immunohistochemistry (IHC)

Tumor samples were obtained from patients presenting to a veterinary hospital with written informed consent (Table S1). The samples were stained with hematoxylin and eosin staining. For IHC, antigens were retrieved in Tris-EDTA buffer (pH 9.0). Tissues were stained with anti-acetylated histone H3 antibody (1:250; #39140, Active Motif, CA, USA) overnight at 4°C and biotinylated goat anti-rabbit IgG (#426012, Nichirei biosciences) for 30 min at RT. The stained slides were scanned with NanoZoomer 2.0-RS (Hamamatsu Photonics, Hamamatsu, Japan) and analyzed with QuPath ver.0.2.1.[33]

2.2 Cell culture

Canine aortic endothelial cells (CnAOEC: #Cn304-05, Cell Applications, CA, USA), seven canine HSA cell lines (JuA1, JuB2, JuB4, Re12, Re21, Ud2, and Ud6),[34] ISOS-1 obtained from the Cell Resource Center for Biomedical Research Cell Bank (Tohoku University),[35] and RAW264 obtained from RIKEN Bioresource Center, were cultured with Dulbecco's Modified Eagle Medium (DMEM; #044-29765, Fujifilm Wako Pure Chemical Industries, Osaka, Japan) supplemented with 10% fetal bovine serum (FBS; #S1580-500, Biowest, UT, USA) and penicillin–streptomycin (#168-23191, Fujifilm Wako) at 37°C with 5% CO_2.

2.3 Drug preparation

SAHA (#10009929, Cayman Chemical, MI, USA) was dissolved in dimethyl sulfoxide (DMSO) to a stock solution of 150 mg/ml. For *in vivo* studies, the stock solution was diluted with 30% polyethylene glycol 400 and 5% Tween 80. VPA (#227-01071, Fujifilm Wako) was dissolved in PBS. JQ1 (#T117580, Toronto Research Chemicals,

Toronto, Canada) was initially dissolved in DMSO to a stock solution of 50 mg/ml. For *in vivo* studies, the stock solution was diluted with 5% Tween 80. Bafilomycin A1 (#554-29211, Fujifilm Wako) was dissolved in DMSO to a stock solution of 1 mM.

2.4 Cell viability assay

Two thousand cells were treated with DMSO or five different concentrations of SAHA or JQ1. Survival rates were analyzed using Cell Counting Kit-8 (CCK-8; #343-07623, Dojindo) and calculated by setting that of DMSO-treated samples as 100%. KyPlot 5.0 software (KyensLab, Inc., Tokyo, Japan) was used to draw survival curves.[36] For growth inhibition curves, the absorbance at the time of treatment (Tz) was measured 24 hours after seeding, and the absorbance at the end of treatment (Ti) was measured 60 hours after treatment. DMSO-treated cells were used as the control (C). Growth inhibition rates were calculated as: [(Ti-Tz)/(C-Tz)] × 100 for concentrations in which Ti>/=Tz, [(Ti-Tz)/Tz] × 100 for concentrations in which Ti < Tz.[37]

2.5 Apoptosis assay

Apoptosis assay was performed using the FITC Annexin V Apoptosis Detection Kit I (#556547, BD Biosciences, NJ, USA) according to the manufacturer's instructions. Briefly, JuB4 and Re12 cells were treated with 10 μM SAHA or JQ1. One million cells were suspended in the binding buffer and stained with annexin V. Cells were analyzed with a BD FACSVerse flow cytometer (BD Biosciences, NJ, USA).

2.6 RNA-Sequencing

ISOS-1 were treated with 1 μM SAHA for 24 h, 1 μM JQ1 for 36 h, or 2 mM VPA for 36 h in triplicate. Total RNA was extracted with a NucleoSpin RNA isolation kit (#740955.50, Macherey-Nagel GmbH & Co. Düren, Germany) according to the manufacturer's instructions. RNA samples were submitted to Kazusa DNA Research Institution (Chiba, Japan) for further analyses. Sequencing reads were mapped to the mm39 mouse reference genome using STAR, and expression levels were estimated using RSEM.[38,39] Differential expression and gene expression profiles were analyzed by edgeR and GSEA v4.1.0, respectively.[40–42]

2.7 SA-β-gal staining

SA-β-gal staining was performed using a Senescence β-Galactosidase Staining Kit (#9860, Cell Signaling Technology, MA, USA) according to the manufacturer's instructions. Briefly, ISOS-1 was treated with DMSO or 10 μM JQ1 for 24 h and fixed with 4% paraformaldehyde (PFA) for 10 min at RT. Cells were stained with β-Galactosidase Staining Solution containing 5-bromo-4-chloro-3-indolyl β-D-galactopyranoside (X-Gal: #16495, Cayman Chemical) for 13 h at 37°C. Positive cells were counted manually using an inverted microscope (BIOREVO BZ-9000; KEYENCE, Tokyo, Japan).

2.8 Cell cycle analysis

ISOS-1, JuB2, JuB4, and Re12 cells were treated with DMSO or JQ1 for 24 hours. ISOS-1 was treated with 10 μM JQ1, and other cell lines were treated with 5 μM JQ1. They

were stained with 30 μM bromodeoxyuridine (BrdU) for 45 min at 37°C, fixed in 70% ethanol overnight and washed with 0.5% Triton X-100 in PBS (PBST). They were resuspended in 500 μL of 2N HCl-0.5% Triton X-100 for 30 min at RT and neutralized with 500 μL of 0.1 M sodium borate buffer (pH 8.5) for 30 min at RT. Then, cells were blocked with 1% bovine serum albumin (BSA, #017-23294, Wako) in PBST for 1 hour. 1.2×10^6 cells were incubated with/without anti-BrdU monoclonal antibody (1:100; MOBU-1 clone, #B35128, Thermo Fisher Scientific) in PBST with 1% BSA for 1 hour at RT and then stained with donkey anti-mouse IgG (H+L) conjugated with AlexaFluor 488 (1:1,000; #A32766, Thermo Fisher Scientific). DNA was stained with 25 μg/ml propidium iodide (PI, #P378, Dojindo). Cell cycle and proliferation were analyzed with BD FACSVerse flow cytometer. Results were analyzed with FCS Express version 4.

2.9 Migration assay

JuB4 and Re12 were treated with DMSO, 2 μM SAHA, or 2 mM VPA for 48 h in 6-well plates. Then, after replacing the medium to the one without inhibitors, the cells were co-cultured with RAW264 seeded on ThinCert Cell Culture Inserts (#657630, Greiner Bio-One) for 24 h. RAW264 on the culture surface of the inserts were removed with a cotton swab. Migrated RAW264 on the bottom side of the inserts were fixed with 4% PFA for 30 min at RT and then stained with 0.01% crystal violet for 30 min at RT. The number of cells was counted manually in 10 fields at 200× under a light microscope (BH-2; Olympus, Tokyo, Japan).

2.10 Western blotting

SDS lysis buffer {2% SDS, 50 mM Tris-HCl (pH6.8), 1 mM EDTA (pH 8.0)} was added to cultured cells or minced tumor tissues after washing them with PBS twice. Cell lysates and the supernatant of the minced tumor tissues were then sonicated using BRANSON Sonifier 450 (Branson Ultrasonics Corporation, CT, USA) for 2 seconds at power 2. 2 μg protein was used for analysis. Primary antibody and secondary antibody reactions were done in Can Get Signal Solution 1 (#NKB-101, TOYOBO, Osaka, Japan) overnight at 4°C in Can Get Signal Solution 2 (TOYOBO) for 1 h at RT. Data were processed using ImageJ.[43] Antibodies used in this study are listed in Table S2.

2.11 Reverse transcription quantitative polymerase chain reaction (RT-qPCR)

Total RNA was extracted with TriPure Isolation Reagent (#11667157001, Roche, Basel, Switzerland). Reverse transcription was performed using Primescript II 1st strand cDNA Synthesis Kit (#6210, Takara Bio, Kusatsu, Japan) for 1 μg total RNA of samples. qPCR was performed using KAPA SYBR FAST qPCR Kit Master Mix (2×) ABI Prism (KK4605, KAPA Biosystems, MA, USA). Primers are listed in Table S3. Results were normalized using the geometric mean of reference genes (*RPL32* and *HPRT* for canine genes, and *Hprt* and *Tbp* for murine genes), which were selected from potential internal controls by geNorm (Fig. S1).[44] Primer efficiencies were between 90% and 110% for all primer sets (Fig. S2). Relative expression levels were calculated by setting the expression levels in the DMSO-treated samples as 1.

2.12 Animal studies

All mouse experiments were performed under the guidelines of an institute, which

follows the ARRIVE guidelines. Five-week-old female Balb/c and KSN/Slc mice (Japan SLC, Inc. Shizuoka, Japan) were used. A day before tumor cell inoculation, KSN/Slc mice were treated with 100 μL 2.5 mg/ml anti-asialo GM1 (#014-09801, Fujifilm Wako) to increase the success rate of JuB2 transplantation.[45] Five million cells were inoculated subcutaneously in both flanks of Balb/c and KSN/Slc mice. Tumor volumes were calculated using the formula: Volume = (Length × Width^2)/2. When the tumor volume reached 100 mm^3, inhibitor treatment was started. Mice were intraperitoneally injected with SAHA (150 mg/kg) daily,[46] VPA (200 mg/kg) five times weekly,[47] or JQ1 (50 mg/kg) daily.[48,49] For preliminary experiments, tumor tissues were collected from three mice for each inhibitor three days after starting treatments and were subject to western blotting or IHC. Comparison in IHC was done among the samples placed on the same slides. For treatment experiments, Balb/c mice were euthanized with CO_2 when tumors reached 1,000 mm^3 in volume. KSN/Slc mice were euthanized with CO_2 11 or 12 days after treatment initiation. Survival times were defined as the period from beginning of drug administration to euthanasia.

2.13 Statistical analysis

Statistical analyses were performed with R (version 4.1.0). Fisher's exact test was used to analyze the ratio of acetylated H3 staining levels. Student's *t*-test or Mann-Whitney test were used to analyze the differences between two groups, whereas Tukey's test was used to analyze differences among multiple groups. Survival curves were analyzed using the log-rank test. Overall tumor growth was analyzed with two-way ANOVA.

3. Results

3.1 Histone acetylation levels in HSA cells are high *in vitro* and heterogeneous *in vivo*

We first analyzed histone acetylation levels in HSA cell lines and CnAOEC. We found that global acetylation of H2B, H3, and H4 was highly enriched in all HSA cell lines compared with CnAOEC (Fig. 1A). Then, we examined global acetylated histone H3 levels in 10 clinical HSA cases. These cases were classified into three types according to their histological pattern: solid, capillary, or cavernous.[1] Five cases had a single histological pattern, while the other five possessed multiple proliferation patterns (Fig, 1B). We also classified histone H3 acetylation levels into three groups based on the normalized values: negative (< 0.5), weak (0.5–2.0), and strong (> 2.0) (Figs. 1C and 1D). The results showed that the histone H3 acetylation levels of tumor cells were heterogeneous, and the ratio was different depending on their histological pattern even in the same tumor tissue (Figs. 1E and 1F). Furthermore, the ratio of tumor cells classified as negative was the highest in the solid pattern followed by the capillary pattern, and the lowest in the cavernous pattern (Fig. 1F). These results suggest that histone H3 acetylation levels are heterogeneous in tumor cells and are associated with their histopathological patterns.

3.2 SAHA and JQ1 induce apoptosis in HSA cell lines

To examine the roles of histone acetylation in HSA, we modified histone acetylation levels using HDACi (SAHA and VPA) and BETi (JQ1) in canine and murine HSA cell lines. First, we evaluated whether global histone acetylation levels were altered by these inhibitors. SAHA and VPA treatments increased global histone acetylation levels in both canine and murine HSA cell lines, whereas JQ1 decreased them in H2B, H3 and H4 of JuB2 and JuB4, in H4 of Re21 and in H2B of ISOS-1 (Fig. 2A). Then, we examined the effects of HDACi and BETi on HSA cell proliferation. SAHA and JQ1 treatment highly decreased the number of cells, while VPA treatment did not affect their proliferation (Figs. 2B and S3A). IC_{50} values

of SAHA and JQ1 in HSA cell lines were almost or less than one-tenth of those in CnAOEC, which indicated that HSA cell lines were more susceptible to these inhibitors than CnAOEC (Fig. 2C). Then, we checked apoptosis markers and found that SAHA and JQ1 increased cleaved caspase 3 expression levels and annexin V positivity in HSA cell lines except for JQ1-treated ISOS-1 (Figs. 2D–F). Neither change was observed in VPA treatment (Figs. 2D, S3B and S3C). Finally, we evaluated protein expression and phosphorylation levels of cell survival proteins AKT and ERK. Although the results were different among the cell lines, either total or phosphorylated AKT or ERK levels were downregulated by SAHA and JQ1 but not by VPA (Fig. S4). These results suggest that SAHA and JQ1 induced apoptosis in HSA cell lines except for ISOS-1 treated with JQ1, and that VPA did not induce cell death in all HSA cell lines.

3.3 SAHA and VPA activate inflammatory responses in HSA cell lines

We further investigated the mechanisms of the effects of the inhibitors in HSA cells. GSEA results indicated that inflammatory-related gene expression was positively correlated in SAHA and VPA treatment in ISOS-1 (Fig. 3A). Consistent with this, *Il6*, *Cxcl1*, *Ccl2*, *Ccl7*, and *Oas1a* were upregulated more than two-fold following treatment with either SAHA or VPA or both (Fig. 3B). We wanted to extrapolate these findings to canine HSA, but *CXCL1* does not exist in the canine genome, *CCL2* expression was not detected, and *CCL7* expression was not increased by SAHA and VPA treatments. However, *OAS1*, the orthologue of murine *Oas1a*, and other inflammatory-related genes were upregulated more than two-fold in canine HSA cell lines treated with SAHA and/or VPA (Fig. 3C). Inflammatory responses in tumor cells can induce immune cell migration, leading to host immune responses to tumor tissues. Therefore, to corroborate whether SAHA and VPA treatment in HSA cell lines can attract immune cells, a macrophage migration assay was performed using RAW264, a mouse

macrophage-like cell line (Fig. 3D). RAW264 migrated when they were co-cultured with SAHA-treated JuB4 or VPA-treated Re12 (Fig. 3E) but not in ISOS-1 (Fig. S5). These results suggest that SAHA and VPA can induce inflammatory responses in canine HSA cell lines. This could attract macrophages, although it depends on the combination of cell lines and HDACi.

3.4 JQ1 induces autophagy and impedes the cell cycle in HSA cell lines

We also investigated the genome-wide gene expression changes in JQ1-treated ISOS-1. GSEA showed that autophagy-related gene expression and cell cycle related-gene expression were positively and negatively correlated, respectively (Figs 4A and 4B). These expression changes were validated by RT-qPCR (Fig. 4C). LC3-II, an active autophagy marker, was expressed at higher levels in all JQ1-treated HSA cell lines except for Re12 compared with DMSO controls (Fig. 4D). Moreover, cotreatment of JQ1 and bafilomycin A1, an inhibitor of autophagosome-lysosome fusion, further enhanced LC3-II expression (Fig. 4D). These results indicated that JQ1 activated initiation of autophagy in HSA cell lines but not inhibited autophagosome degradation.

Although JQ1 treatment in ISOS-1 deceased cell viability, it did not increase apoptosis marker expressions (Figs. 2C-F). These results led us to speculate that JQ1 retarded cell proliferation but not actively induced cell death. To clarify this speculation, we generated growth inhibition curves through which we could evaluate whether the cells actively died or slowed their proliferation speed by JQ1 in ISOS-1. The results showed that growth inhibition rates were positive even when the cells were treated with 10 μM JQ1, which indicated that JQ1 mainly led to cell cycle delay in ISOS-1 (Fig. 5A). Then, we further evaluated cell cycle status under JQ1 treatment in ISOS-1 and canine HSA cell lines. BrdU and propidium iodide (PI) staining revealed that proliferating cells (BrdU+ cells) were significantly decreased in

both murine and canine HSA cell lines by JQ1 (Fig. 5B). PI signals showed that the percentage of dead cells was slightly increased by JQ1 in ISOS-1, but its extent was lower than in canine HSA cell lines (Fig. 5C). We also examined cell senescence by performing SA-β-gal staining in ISOS-1 cells. The results indicated that JQ1-treated ISOS-1 showed a significantly higher number of positive cells than DMSO-treated cells (Fig. 5D).

These results suggest that autophagy activation and cell cycle downregulation are induced by JQ1, and that cell cycle retardation and cell senescence are major effects of JQ1 in ISOS-1.

3.5 JQ1 suppresses HSA tumor growth *in vivo*

Finally, to evaluate the treatment effects of SAHA, VPA, and JQ1 *in vivo*, we treated ISOS-1 tumor-bearing Balb/c mice with SAHA, VPA, or JQ1. Three days SAHA and VPA treatment increased global acetylated H3 levels in tumor tissues (Fig. S6A). Quantitative IHC analysis revealed that global acetylated histone H3 levels in tumor cells were slightly increased in SAHA and VPA treatments, whereas they were decreased in JQ1 treatments (Figs. S6B - S6D). VPA treatments altered staining patterns in the nuclei of tumor cells compared with the DMSO control (Fig. S6C, insets). Long term treatment experiments revealed that only JQ1 slowed tumor growth and extended median and mean survival times by 6 days and 5.6 days, respectively (Fig. 6A and B). JQ1 treatment in JuB2 tumor-bearing KSN/Slc mice also suppressed JuB2 tumor growth (Fig. 6C). These treatments did not cause body weight loss in mice (Fig. S7). These results suggest that JQ1 has suppressive effects on HSA tumor growth *in vivo*.

4. Discussion

HSA tumor cells in clinical cases showed various H3 acetylation levels even in the

same tumor tissue. Moreover, this heterogeneity differed depending on the histological pattern. These results can be explained by the differentiation status of the tumor cells. Global histone acetylation levels have been reported to be increased as cells differentiate.[50,51] Furthermore, HSA tumor cells forming the solid pattern are considered to be undifferentiated.[52] Given that the percentage of tumor cells classified as H3 acetylation-negative was high in the solid pattern, they could be more undifferentiated than other tumor cells. Further research is required to clarify whether global histone acetylation levels reflect the differentiation status of HSA tumor cells.

We demonstrated that SAHA and VPA upregulated inflammatory-related genes and attracted RAW264 cells in JuB4 or Re12 cells. *OAS1* and *OAS2*, genes upregulated by SAHA and VPA in canine HSA cells, are interferon-stimulated genes (ISGs).[53] Increased ISGs result in tumor regression by turning immunologically cold tumors hot, thereby attracting anti-tumor immune cells into tumor tissues. [54,55] Several reports indicated that HDACi activated immune responses and enhanced immune cell functions.[56–58] According to these findings, HSA cells could also gain anti-tumor effects by HDACi treatment. However, other upregulated genes in our study, *CXCL8* and *CXCL12*, have been reported to promote tumor progression by several mechanisms such as inducing angiogenesis or polarizing macrophages to an M2 state.[59–61] Furthermore, given that a recent report demonstrated that a large numbers of M2-polarized macrophages exist in HSA tumor tissues and HSA cells could induce M2 polarization in macrophages,[32] HDACi might promote HSA tumor progression by upregulating the expression of tumor-promoting cytokines such as *CXCL8* and *CXCL12*. Further research is required to understand the effects of HDACi on tumor immunity.

In our study, SAHA and VPA did not either suppress or promote tumor growth of ISOS-1 in an immunocompetent mouse model. This is explained by several possibilities. First, histone deacetylases functioning in ISOS-1, which can be targeted by HDACi, might

differ from *in vitro* to *in vivo* conditions. Thus, HDACi effects might differ depending on the experimental conditions. Second, the plasma concentrations of the drugs might be decreased too fast to induce anti-tumor effects. In our experiment, global histone H3 acetylation levels were only slightly increased by SAHA and VPA, although we referred to previous reports to determine the dose (Fig. S6).[46–49] SAHA has been noted for its fast reduction in plasma concentration in *in vivo* models.[62] Third, the conditions we tested did not induce anti-tumor immune responses. Co-treatment with other drugs such as doxorubicin or immune checkpoint inhibitors would be beneficial for HSA treatment by stimulating immune responses.[63–66] Further research is required to investigate whether SAHA and VPA can be used as alternative therapeutics in HSA.

In our study, JQ1 induced apoptosis, autophagy initiation, and tumor growth suppression in canine HSA cells. Apoptosis is probably related to tumor growth suppression, but no clear answer about whether autophagy had anti- or pro-tumor effects was obtained from our study. This is because autophagy has two opposite roles in tumor cells: cytoprotective and cytotoxic.[67] In ovarian cancer and acute myeloid leukemia in humans, JQ1-induced autophagy had a cytoprotective role and an autophagy inhibitor enhanced the anti-tumor effect of JQ1. [68,69] Conversely, in human bladder cancer cell lines, the proliferation suppression capacity of JQ1 was attenuated by autophagy inhibitors, which suggested that JQ1-induced autophagy had a cytotoxic role.[23] Further experiments are needed to elucidate which roles JQ1-induced autophagy has in HSA.

Although the autophagy effects induced by JQ1 were not clear in our study, JQ1 suppressed tumor growth in both canine and murine HSA cell lines *in vivo*. JQ1 treatment did not alter global histone H3 acetylation levels in tumor tissues, but those in tumor cells were moderately decreased (Fig. S5). Several reports indicated that JQ1 induced minor changes in histone marks but inhibited BET proteins, reader proteins for histone acetylation.[70–74] To

further understand how JQ1 affects tumor growth *in vivo,* local histone acetylation levels must be investigated by chromatin immunoprecipitation (ChIP) or by the cleavage under targets and release using nuclease (CUT&RUN) technique using tumor tissues treated with JQ1. Several reports revealed that JQ1 or other BETis had anti-tumor effects, and clinical trials were conducted in lymphoma, prostate cancer, and solid tumors.[24,75] Moreover, oral BETis molibresib and INCB054329 induced tumor suppression in clinical and *in vivo* studies.[76,77] Although further research is required, our results suggest that BETis could be an alternative therapeutic for canine HSA.

In conclusion, we demonstrated that BETis can be used for HSA treatment. Although further research is required, our results suggest that dysregulation of histone acetylation is likely to be involved in HSA malignancy.

References

1. Kim JH, Graef AJ, Dickerson EB, Modiano JF. Pathobiology of hemangiosarcoma in dogs: Research advances and future perspectives. *Vet Sci* 2015;2(4):388–405.
2. Clifford CA, Mackin AJ, Henry CJ. Treatment of canine hemangiosarcoma: 2000 and beyond. *J Vet Intern Med* 2000;14(5):479–485.
3. Shustef E, Kazlouskaya V, Prieto VG, Ivan D, Aung PP. Cutaneous angiosarcoma: A current update. *J Clin Pathol* 2017;70(11):917–925.
4. Leduc C, Jenkins SM, Sukov WR, Rustin JG, Maleszewski JJ. Cardiac angiosarcoma: histopathologic, immunohistochemical, and cytogenetic analysis of 10 cases. *Hum Pathol* 2017;60:199–207.
5. Megquier K, Turner-Maier J, Swofford R, et al. Comparative genomics reveals shared mutational landscape in canine hemangiosarcoma and human angiosarcoma. *Mol Cancer Res* 2019;17(12):2410–2421.

6. Kaelin WG, McKnight SL. Influence of metabolism on epigenetics and disease. *Cell* 2013;153(1):56–69.
7. Virani S, Virani S, Colacino JA, Kim JH, Rozek LS. Cancer epigenetics: a brief review. *ILAR J*;53(3–4):359–369.
8. Xu R, Li C, Liu X, Gao S. Insights into epigenetic patterns in mammalian early embryos. *Protein Cell* 2021;12(1):7–28.
9. Josling GA, Selvarajah SA, Petter M, Duffy MF. The role of bromodomain proteins in regulating gene expression. *Genes (Basel)* 2012;3(2):320–343.
10. Clayton AL, Hazzalin CA, Mahadevan LC. Enhanced histone acetylation and transcription: A dynamic perspective. *Mol Cell* 2006;23(3):289–296.
11. Calcagno DQ, Wisnieski F, Da Silva Mota ER, et al. Role of histone acetylation in gastric cancer: Implications of dietetic compounds and clinical perspectives. *Epigenomics* 2019;11(3):349–362.
12. Liu KY, Wang LT, Hsu SH. Modification of epigenetic histone acetylation in hepatocellular carcinoma. *Cancers (Basel)* 2018;10(1):8.
13. West AC, Johnstone RW. New and emerging HDAC inhibitors for cancer treatment. *J Clin Invest* 2014;124(1):30–39.
14. Bechter O, Schöffski P. Make your best BET: The emerging role of BET inhibitor treatment in malignant tumors. *Pharmacol Ther* 2020;208:107479.
15. Claerhout S, Lim JY, Choi W, et al. Gene expression signature analysis identifies vorinostat as a candidate therapy for gastric cancer. *PLoS One* 2011;6(9):e24662.
16. Lee YJ, Won AJ, Lee J, et al. Molecular mechanism of SAHA on regulation of autophagic cell death in tamoxifen-resistant MCF-7 breast cancer cells. *Int J Med Sci* 2012;9(10):881–893.
17. Uehara N, Kanematsu S, Miki H, Yoshizawa K, Tsubura A. Requirement of p38

MAPK for a cell-death pathway triggered by vorinostat in MDA-MB-231 human breast cancer cells. *Cancer Lett* 2012;315(2):112–121.

18. Yagi Y, Fushida S, Harada S, et al. Effects of valproic acid on the cell cycle and apoptosis through acetylation of histone and tubulin in a scirrhous gastric cancer cell line. *J Exp Clin Cancer Res* 2010;29(1):149.

19. Gameiro SR, Malamas AS, Tsang KY, Ferrone S, Hodge JW. Inhibitors of histone deacetylase 1 reverse the immune evasion phenotype to enhance T-cell mediated lysis of prostate and breast carcinoma cells. *Oncotarget* 2016;7(7):7390–7402.

20. Kortenhorst MS, Wissing MD, Rodríguez R, et al. Analysis of the genomic response of human prostate cancer cells to histone deacetylase inhibitors. *Epigenetics* 2013;8(9):907–920.

21. Xue K, Gu JJ, Zhang Q, et al. Vorinostat, a histone deacetylase (HDAC) inhibitor, promotes cell cycle arrest and re-sensitizes rituximab- and chemo-resistant lymphoma cells to chemotherapy agents. *J Cancer Res Clin Oncol* 2016;142(2):379–387.

22. Jostes S, Nettersheim D, Fellermeyer M, et al. The bromodomain inhibitor JQ1 triggers growth arrest and apoptosis in testicular germ cell tumours in vitro and in vivo. *J Cell Mol Med* 2017;21(7):1300–1314.

23. Li F, Yang C, Zhang HB, et al. BET inhibitor JQ1 suppresses cell proliferation via inducing autophagy and activating LKB1/AMPK in bladder cancer cells. *Cancer Med* 2019;8(10):4792–4805.

24. Wen N, Guo B, Zheng H, et al. Bromodomain inhibitor jq1 induces cell cycle arrest and apoptosis of glioma stem cells through the VEGF/PI3K/AKT signaling pathway. *Int J Oncol* 2019;55(4):879–895.

25. Gulay KCM, Aoshima K, Shibata Y, et al. KDM2B promotes cell viability by enhancing DNA damage response in canine hemangiosarcoma. *J Genet Genomics*

2021;48(7):618–630.

26. Galli F, Aguilera JV, Palermo B, Markovic SN, Nisticò P, Signore A. Relevance of immune cell and tumor microenvironment imaging in the new era of immunotherapy. *J Exp Clin Cancer Res* 2020;39:89.

27. Sun X, Fu X, Xu S, et al. OLR1 is a prognostic factor and correlated with immune infiltration in breast cancer. *Int Immunopharmacol* 2021;101 :108275.

28. Xia L, Oyang L, Lin J, et al. The cancer metabolic reprogramming and immune response. *Mol Cancer* 2021;20(1):1–21.

29. Salemme V, Centonze G, Cavallo F, Defilippi P, Conti L. The crosstalk between tumor cells and the immune microenvironment in breast cancer: Implications for immunotherapy. *Front Oncol* 2021;11:289.

30. Lian X, Yang K, Li R, et al. Immunometabolic rewiring in tumorigenesis and anti-tumor immunotherapy. *Mol Cancer* 2022;21(1):1–17.

31. Ghahremani MF, Radaelli E, Haigh K, et al. Loss of autocrine endothelial-derived VEGF significantly reduces hemangiosarcoma development in conditional p53-deficient mice. *Cell Cycle* 2014;13(9):1502–1508.

32. Gulay KCM, Aoshima K, Maekawa N, et al. Hemangiosarcoma cells induce M2 polarization and PD-L1 expression in macrophages. *Sci Rep* 2022;12:2124.

33. Bankhead P, Loughrey MB, Fernández JA, et al. QuPath: Open source software for digital pathology image analysis. *Sci Rep* 2017;7(1):16878.

34. Murai A, Asa SA, Kodama A, Hirata A, Yanai T, Sakai H. Constitutive phosphorylation of the mTORC2/Akt/4E-BP1 pathway in newly derived canine hemangiosarcoma cell lines. *BMC Vet Res* 2012;8:128.

35. Masuzawa M, Fujimura T, Tsubokawa M, et al. Establishment of a new murine-phenotypic angiosarcoma cell line (ISOS-1). *J Dermatol Sci* 1998;16(2) :91–98.

36. Yoshioka K. KyPlot as a tool for graphical data analysis. In:Härdle W, Önz B, eds. Compstat. Physica, Heidelberg 2002;37–46.
37. National institutes of health. NCI-60 screening methodology. 2021. https://dtp.cancer.gov/discovery_development/nci-60/methodology.htm. Accessed Oct. 21. 2021.
38. Dobin A, Gingeras TR. Mapping RNA-seq reads with STAR. *Curr Protoc Bioinforma* 2015;51(1):11.14.1-11.14.19.
39. Li B, Dewey CN. RSEM: Accurate transcript quantification from RNA-Seq data with or without a reference genome. *BMC Bioinformatics* 2011;12:323.
40. Robinson MD, McCarthy DJ, Smyth GK. edgeR: A Bioconductor package for differential expression analysis of digital gene expression data. 2009;26(1):139–140.
41. Mootha VK, Lindgren CM, Eriksson KF, et al. PGC-1α-responsive genes involved in oxidative phosphorylation are coordinately downregulated in human diabetes. *Nat Genet* 2003;34(3):267–273.
42. Subramanian A, Tamayo P, Mootha VK, et al. Gene set enrichment analysis: A knowledge-based approach for interpreting genome-wide expression profiles. *Proc Natl Acad Sci U S A* 2005;102(43):15545–15550.
43. Schneider CA, Rasband WS, Eliceiri KW. NIH image to ImageJ: 25 years of image analysis. *Nat Methods* 2012;9(7):671–675.
44. Vandesompele J, De Preter K, Pattyn F, et al. Accurate normalization of real-time quantitative RT-PCR data by geometric averaging of multiple internal control genes. *Genome Biol* 2002;3(7):research0034.1–0034.11.
45. Yoshino H, Ueda T, Kawahata M, et al. Natural killer cell depletion by anti-asialo GM1 antiserum treatment enhances human hematopoietic stem cell engraftment in NOD/Shi-scid mice. *Bone Marrow Transplant* 2000;26(11):1211–1216.

492 46. Eto S, Saeki K, Yoshitake R, et al. Anti-tumor effects of the histone deacetylase
493 inhibitor vorinostat on canine urothelial carcinoma cells. *PLoS One*
494 2019;14(6):e0218382.
495 47. Terranova-Barberio M, Roca MS, Zotti AI, et al. Valproic acid potentiates the
496 anticancer activity of capecitabine in vitro and in vivo in breast cancer models via
497 induction of thymidine phosphorylase expression. *Oncotarget* 2016;7(7):7715.
498 48. Qiu H, Jackson AL, Kilgore JE, et al. JQ1 suppresses tumor growth through
499 downregulating LDHA in ovarian cancer. *Oncotarget* 2015;6(9):6915–6930.
500 49. Zhu X, Enomoto K, Zhao L, et al. Bromodomain and extraterminal protein inhibitor
501 JQ1 suppresses thyroid tumor growth in a mouse model. *Clin Cancer Res*
502 2017;23(2):430–440.
503 50. Ashktorab H, Belgrave K, Hosseinkhah F, et al. Global histone H4 acetylation and
504 HDAC2 expression in colon adenoma and carcinoma. *Dig Dis Sci* 2009;54(10):2109–
505 2117.
506 51. Golob JL, Paige SL, Muskheli V, Pabon L, Murry CE. Chromatin remodeling during
507 mouse and human embryonic stem cell differentiation. *Dev Dyn* 2008;237(5):1389–
508 1398.
509 52. Göritz M, Müller K, Krastel D, et al. Canine splenic haemangiosarcoma: Influence of
510 metastases, chemotherapy and growth pattern on post-splenectomy survival and
511 expression of angiogenic factors. *J Comp Pathol* 2013;149(1):30–39.
512 53. Justesen J, Hartmann R, Kjeldgaard NO. Gene structure and function of the 2'-5'-
513 oligoadenylate synthetase family. *Cell Mol Life Sci* 2000;57(11):1593–1612.
514 54. Sheng W, LaFleur MW, Nguyen TH, et al. LSD1 ablation stimulates anti-tumor
515 immunity and enables checkpoint blockade. *Cell* 2018;174(3):549-563.e19.
516 55. Zhang SM, Cai WL, Liu X, et al. KDM5B promotes immune evasion by recruiting

SETDB1 to silence retroelements. *Nature* 2021;598(7882):682–687.

56. Cox DJ, Coleman AM, Gogan KM, et al. Inhibiting histone deacetylases in human macrophages promotes glycolysis, IL-1β, and T helper cell responses to mycobacterium tuberculosis. *Front Immunol* 2020;11:1609.

57. Laengle J, Kabiljo J, Hunter L, et al. Histone deacetylase inhibitors valproic acid and vorinostat enhance trastuzumab-mediated antibody-dependent cell-mediated phagocytosis. *J Immunother Cancer* 2020;8(1):e000195.

58. Sun T, Li Y, Yang W, et al. Histone deacetylase inhibition up-regulates MHC class I to facilitate cytotoxic T lymphocyte-mediated tumor cell killing in glioma cells. *J Cancer* 2019;10(23):5638–5645.

59. Xiong X, Liao X, Qiu S, et al. CXCL8 in tumor biology and its implications for clinical translation. *Front Mol Biosci* 2022;9:235.

60. Guo F, Wang Y, Liu J, Mok SC, Xue F, Zhang W. CXCL12/CXCR4: A symbiotic bridge linking cancer cells and their stromal neighbors in oncogenic communication networks. *Oncogene* 2016;35(7):816–826.

61. Babazadeh S, Nassiri SM, Siavashi V, Sahlabadi M, Hajinasrollah M, Zamani-Ahmadmahmudi M. Macrophage polarization by MSC-derived CXCL12 determines tumor growth. *Cell Mol Biol Lett* 2021;26(1):1–15.

62. Fournel M, Bonfils C, Hou Y, et al. MGCD0103, a novel isotype-selective histone deacetylase inhibitor, has broad spectrum antitumor activity in vitro and in vivo. *Mol Cancer Ther* 2008;7(4):759–768.

63. Le DT, Durham JN, Smith KN, et al. Mismatch repair deficiency predicts response of solid tumors to PD-1 blockade. *Science* 2017;357(6349):409–413.

64. Tubbs A, Nussenzweig A. Endogenous DNA damage as a source of genomic instability in cancer. *Cell*;168(4):644–656.

65. Igase M, Nemoto Y, Itamoto K, et al. A pilot clinical study of the therapeutic antibody against canine PD-1 for advanced spontaneous cancers in dogs. *Sci Rep* 2020;10(1):18311.
66. Maekawa N, Konnai S, Takagi S, et al. A canine chimeric monoclonal antibody targeting PD-L1 and its clinical efficacy in canine oral malignant melanoma or undifferentiated sarcoma. *Sci Rep* 2017;7(1):8951.
67. Gewirtz DA. The four faces of autophagy: Implications for cancer therapy. *Cancer Res* 2014;74(3):647–651.
68. Luan W, Pang Y, Li R, et al. Akt/mTOR-mediated autophagy confers resistance to bet inhibitor JQ1 in ovarian cancer. *Onco Targets Ther* 2019;12:8063–8074.
69. Jang JE, Eom JI, Jeung HK, et al. AMPK-ULK1-mediated autophagy confers resistance to BET inhibitor JQ1 in acute myeloid leukemia stem cells. *Clin Cancer Res* 2017;23(11):2781–2794.
70. Rathert P, Roth M, Neumann T, et al. Transcriptional plasticity promotes primary and acquired resistance to BET inhibition. *Nature* 2015;525(7570):543–547.
71. Shu S, Lin CY, He HH, et al. Response and resistance to BET bromodomain inhibitors in triple-negative breast cancer. *Nature* 2016;529(7586):413–417.
72. Kanno T, Kanno Y, Leroy G, et al. BRD4 assists elongation of both coding and enhancer RNAs by interacting with acetylated histones. *Nat Struct Mol Biol* 2014;21(12):1047–1057.
73. Najafova Z, Tirado-Magallanes R, Subramaniam M, et al. BRD4 localization to lineage-specific enhancers is associated with a distinct transcription factor repertoire. *Nucleic Acids Res* 2017;45(1):127–141.
74. Kedaigle AJ, Reidling JC, Lim RG, et al. Treatment with JQ1, a BET bromodomain inhibitor, is selectively detrimental to R6/2 Huntington's disease mice. *Hum Mol Genet*

2020;29(2):202–215.

75. Shorstova T, Foulkes WD, Witcher M. Achieving clinical success with BET inhibitors as anti-cancer agents. *Br J Cancer* 2021;124(9):1478–1490.

76. Cousin S, Blay JY, Garcia IB, et al. Safety, pharmacokinetic, pharmacodynamic and clinical activity of molibresib for the treatment of nuclear protein of the testis carcinoma and other cancers: Results of a Phase I/II open-label, dose escalation study. *Int J Cancer* 2022;150(6):993–1006.

77. Stubbs MC, Burn TC, Sparks R, et al. The novel bromodomain and extraterminal domain inhibitor INCB054329 induces vulnerabilities in myeloma cells that inform rational combination strategies. *Clin Cancer Res* 2019;25(1):300–311.

Figure legends

Fig 1. Histone acetylation levels in HSA cells are high *in vitro* and heterogenous *in vivo.*

(A) Western blot analysis of acetylated histone H2B, H3, and H4. (B) Representative images of HE and IHC staining in clinical HSA cases. Scale bars = 50 μm. (C) Box plots for normalized nucleus DAB OD mean values in 10 clinical HSA cases. (D) Representative IHC images of the classifications according to normalized acetylated H3 intensities in each histological pattern. Arrowheads indicate the nuclei of tumor cells. (E) Stacked bar graphs indicating the ratio of each staining level in 10 clinical cases. (F) Stacked bar graphs comparing the ratio of each staining level according to the histological patterns in all cases or within each case. *$P < 0.05$, **$P < 0.01$. Fisher's exact test.

Fig 2. SAHA and JQ1 induce apoptosis in HSA cell lines.

(A) Western blot analysis of acetylated H2B, H3, and H4 in canine HSA cell lines (JuB2, JuB4, Re12) and a murine HSA cell line (ISOS-1) treated with DMSO, SAHA, JQ1, or VPA.

(B) Phase contrast images of canine and murine HSA cell lines 48 h after treatment with DMSO, SAHA, VPA, or JQ1. Scale bars = 100 μm. (C) Survival curves (top) and IC_{50} values (bottom) of canine and murine HSA cell lines treated with SAHA or JQ1 for 60 h. All samples were analyzed in triplicate. Data are plotted as average percentages ± SD. (D) Western blot analysis of cleaved caspase 3 in canine and murine HSA cells treated with DMSO, SAHA, VPA, or JQ1. (E) Annexin V staining of canine and murine HSA cells treated with DMSO, SAHA, or JQ1. (F) Percentages of apoptotic cells (annexin V-positive) in canine and murine HSA cells treated with DMSO, SAHA, or JQ1. All samples were analyzed in triplicate. Data are plotted as average percentages ± SD. *$P < 0.05$, **$P < 0.01$. Tukey's test.

Fig 3. SAHA and VPA activate inflammatory responses in HSA cell lines.

(A) (Left) GSEA results in ISOS-1 treated with SAHA (top) or VPA (bottom). Inflammatory-related gene sets are highlighted in red. The number of genes in each gene set is shown next to each bar. (Right) Representative GSEA plots of enriched gene sets in ISOS-1 treated with SAHA (top) or VPA (bottom). (B) RT-qPCR results of genes related to inflammatory responses in ISOS-1 treated with SAHA or VPA. (C) RT-qPCR results of inflammatory-related genes in JuB4 and Re12 treated with SAHA or VPA. (D) Graphical images of migration assay. (E) Quantitative analysis of migrated RAW264 cells co-cultured with SAHA or VPA-treated Re12. Data are plotted as average percentages ± SD. *$P < 0.05$, **$P < 0.01$. Tukey's test.

Fig 4. JQ1 treatment induces autophagy in canine and murine HSA cell lines.

(A) Positively (top) or negatively (bottom) enriched gene sets by GSEA in ISOS-1 treated with JQ1 compared with DMSO-treated cells. The number of genes in each gene set is shown next to each bar. (B) Representative GSEA plots of positively (top) and negatively (bottom)

enriched gene sets. (C) RT-qPCR of genes related to autophagy (top) and cell cycle (bottom) in ISOS-1 treated with DMSO or JQ1. (D) Western blot analysis for LC3 expression in canine and murine HSA cell lines treated with DMSO, JQ1 (10 μM, 24 hours) and/or bafilomycin A1(100 nM, 3 hours). Data are plotted as average percentages ± SD.

Fig. 5. JQ1 treatment impedes the cell cycle in canine and murine HSA cell lines.
(A) A growth inhibition curve of ISOS-1 treated with JQ1. All samples were analyzed in triplicate. Data are plotted as average percentages ± SD. (B) Density plots (left) and quantitative analysis (right) of BrdU-positive cells in canine and murine HSA cell lines treated with DMSO or JQ1. All samples were analyzed in triplicate. (C) Histograms of PI-positive cells (left) and quantitative analysis of dead cells (right) in canine and murine HSA cell lines treated with DMSO and JQ1. All samples were analyzed in triplicate. (D) (Left) Representative images of SA-β-gal staining in ISOS-1 treated with DMSO or JQ1. Arrowheads indicate positive cells. (Right) Quantitative analysis of SA-β-gal-positive cells. Positive cells were counted in 10 fields under 200× magnification with a light microscope. The average numbers were plotted with ± SD. Scale bars = 100 μm. $*P < 0.05$, $**P < 0.01$. Student's *t*-test.

Fig 6. JQ1 suppresses HSA tumor growth *in vivo.*
(A) Kaplan–Meier survival curves of ISOS-1-inoculated Balb/c mice treated with DMSO (n=5), SAHA (n=5), VPA (n=4), or JQ1 (n=5). Days were counted after initiating drug treatment. *P*-values were calculated using the log-rank test. (B) Individual growth curves of ISOS-1 tumors in Balb/c mice treated with DMSO, SAHA, VPA, or JQ1 after treatment initiation. (C) (Left) Individual tumor growth curves of JuB2 tumors in KSN/Slc mice treated with DMSO or JQ1. The day when the treatment began was defined as day 1. $***P < 0.001$.

642 Two-way ANOVA. (Right) Box plots of relative tumor volumes on the last day in KSN/Slc
643 mice treated with DMSO or JQ1. Relative tumor volumes were calculated by dividing the
644 tumor volume on the last day by that at day 1. *$P < 0.05$, Mann-whitney U test.

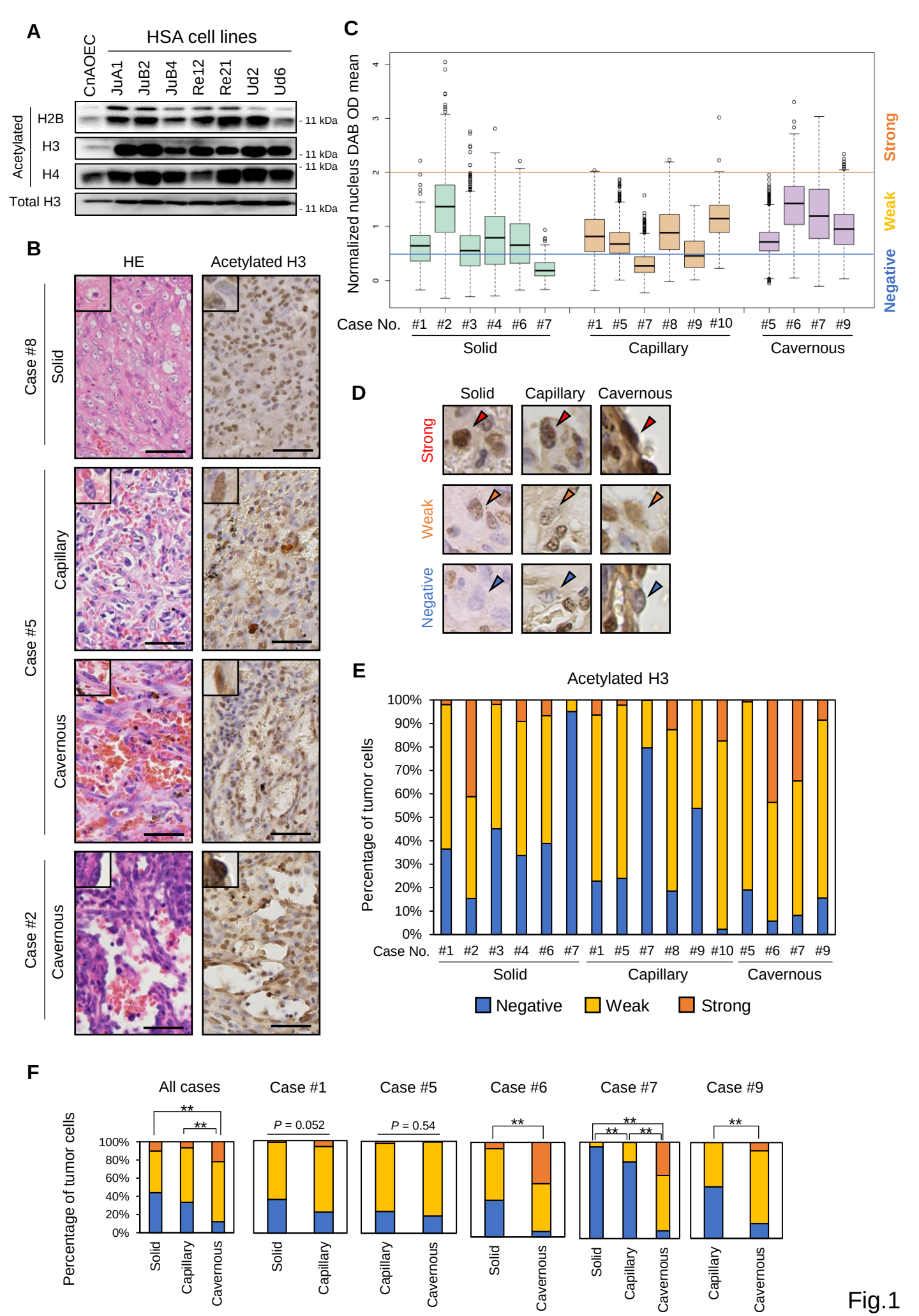
A
HSA cell lines
CnAOEC
JuA1
JuB2
JuB4
Re12
Re21
Ud2
Ud6
Acetylated
H2B
H3
H4
Total H3
11 kDa
B
HE
Acetylated H3
Case #8
Solid
Case #5
Capillary
Cavernous
Case #2
Cavernous
C
Normalized nucleus DAB OD mean
Negative
Weak
Strong
Case No. #1 #2 #3 #4 #6 #7 #1 #5 #7 #8 #9 #10 #5 #6 #7 #9
Solid
Capillary
Cavernous
D
Solid
Capillary
Cavernous
Strong
Weak
Negative
E
Acetylated H3
Percentage of tumor cells
100%
90%
80%
70%
60%
50%
40%
30%
20%
10%
0%
Case No. #1 #2 #3 #4 #6 #7 #1 #5 #7 #8 #9 #10 #5 #6 #7 #9
Solid
Capillary
Cavernous
Negative
Weak
Strong
F
All cases
Case #1
Case #5
Case #6
Case #7
Case #9
Percentage of tumor cells
100%
80%
60%
40%
20%
0%
**
P = 0.052
P = 0.54
Solid
Capillary
Cavernous

Fig.1

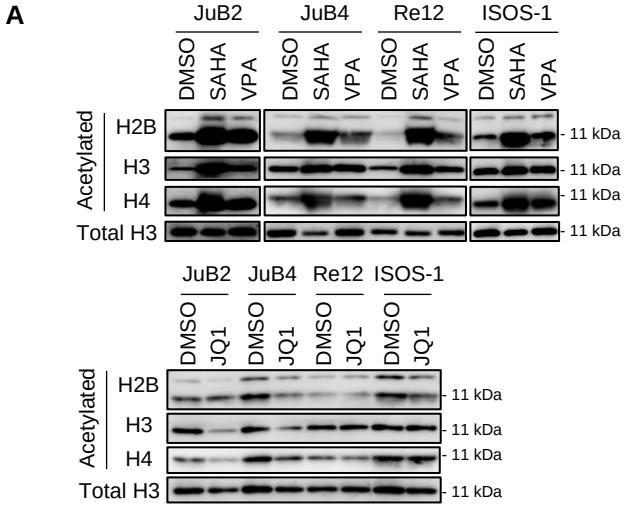

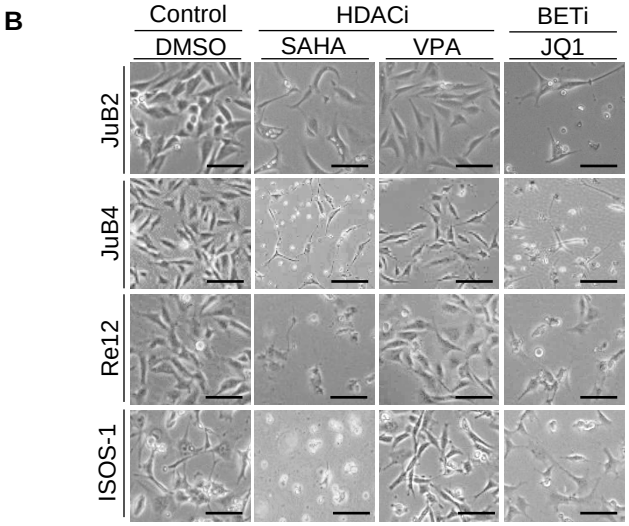

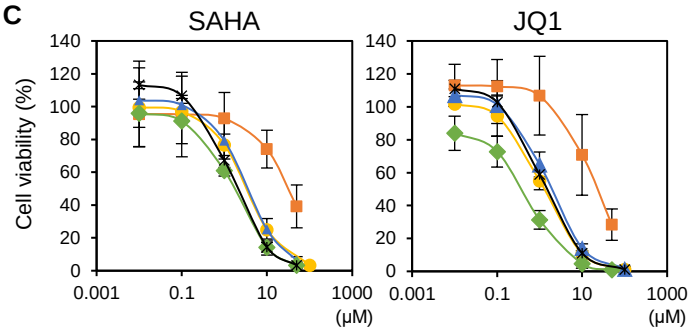

Cell line	SAHA IC_{50} (μM)	JQ1 IC_{50} (μM)
CnAOEC	31.60	21.10
JuB2	3.30	1.22
JuB4	3.47	1.75
Re12	1.61	0.41
ISOS-1	1.84	1.37

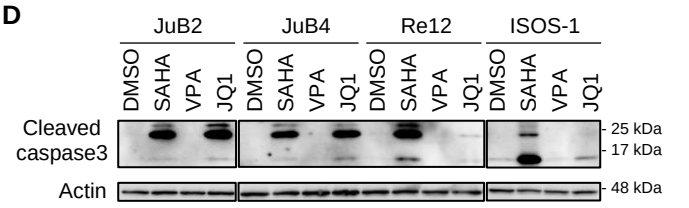

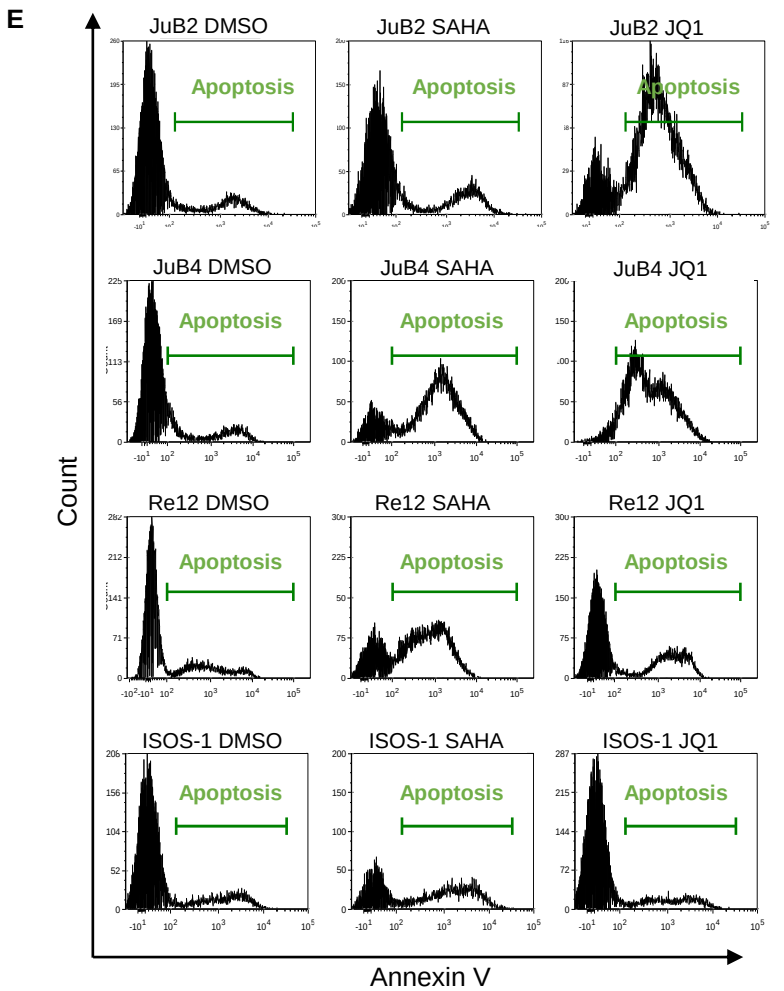

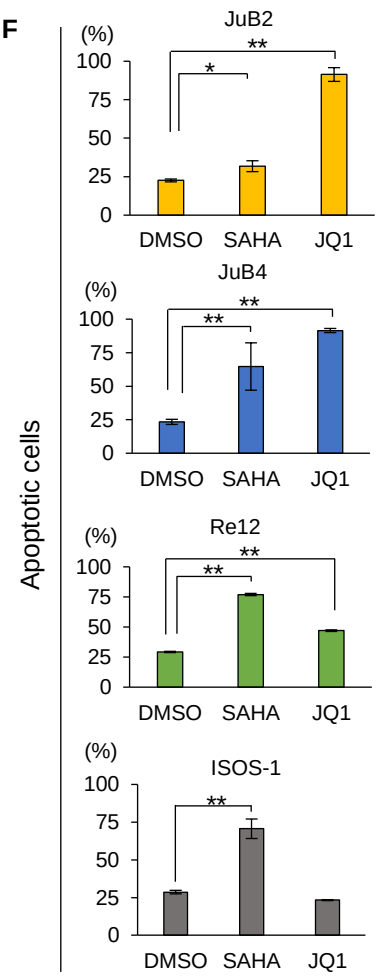

Fig.2

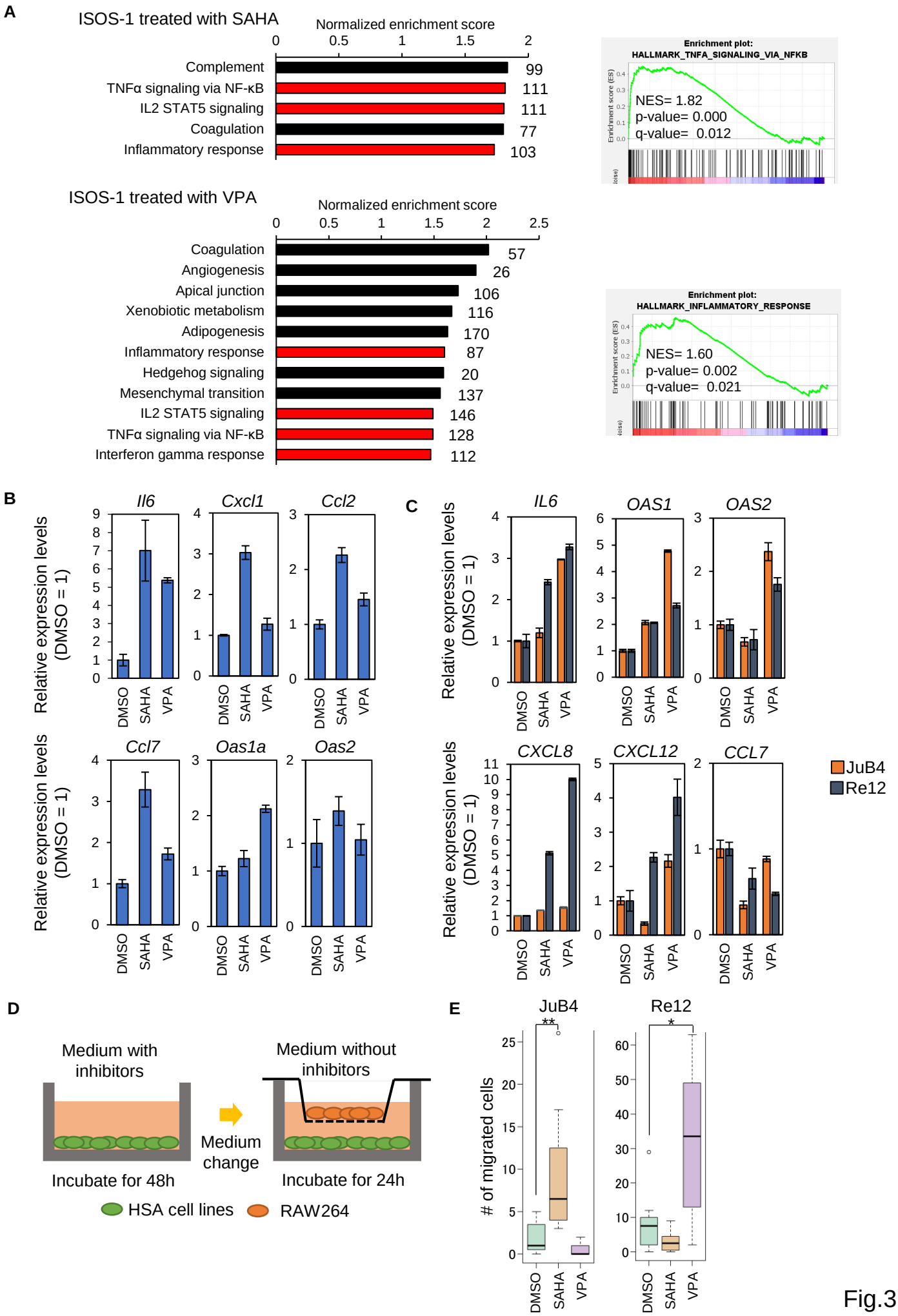
A
ISOS-1 treated with SAHA
Normalized enrichment score
0
0.5
1
1.5
2
Complement
TNFα signaling via NF-κB
IL2 STAT5 signaling
Coagulation
Inflammatory response
99
111
111
77
103
Enrichment plot:
HALLMARK_TNFA_SIGNALING_VIA_NFKB
NES= 1.82
p-value= 0.000
q-value= 0.012
ISOS-1 treated with VPA
Normalized enrichment score
0
0.5
1
1.5
2
2.5
Coagulation
Angiogenesis
Apical junction
Xenobiotic metabolism
Adipogenesis
Inflammatory response
Hedgehog signaling
Mesenchymal transition
IL2 STAT5 signaling
TNFα signaling via NF-κB
Interferon gamma response
57
26
106
116
170
87
20
137
146
128
112
Enrichment plot:
HALLMARK_INFLAMMATORY_RESPONSE
NES= 1.60
p-value= 0.002
q-value= 0.021
B
Il6
Cxcl1
Ccl2
Ccl7
Oas1a
Oas2
Relative expression levels
(DMSO = 1)
DMSO
SAHA
VPA
C
IL6
OAS1
OAS2
CXCL8
CXCL12
CCL7
JuB4
Re12
D
Medium with inhibitors
Medium without inhibitors
Medium change
Incubate for 48h
Incubate for 24h
HSA cell lines
RAW264
E
JuB4
Re12
# of migrated cells
**
*
DMSO
SAHA
VPA

Fig.3

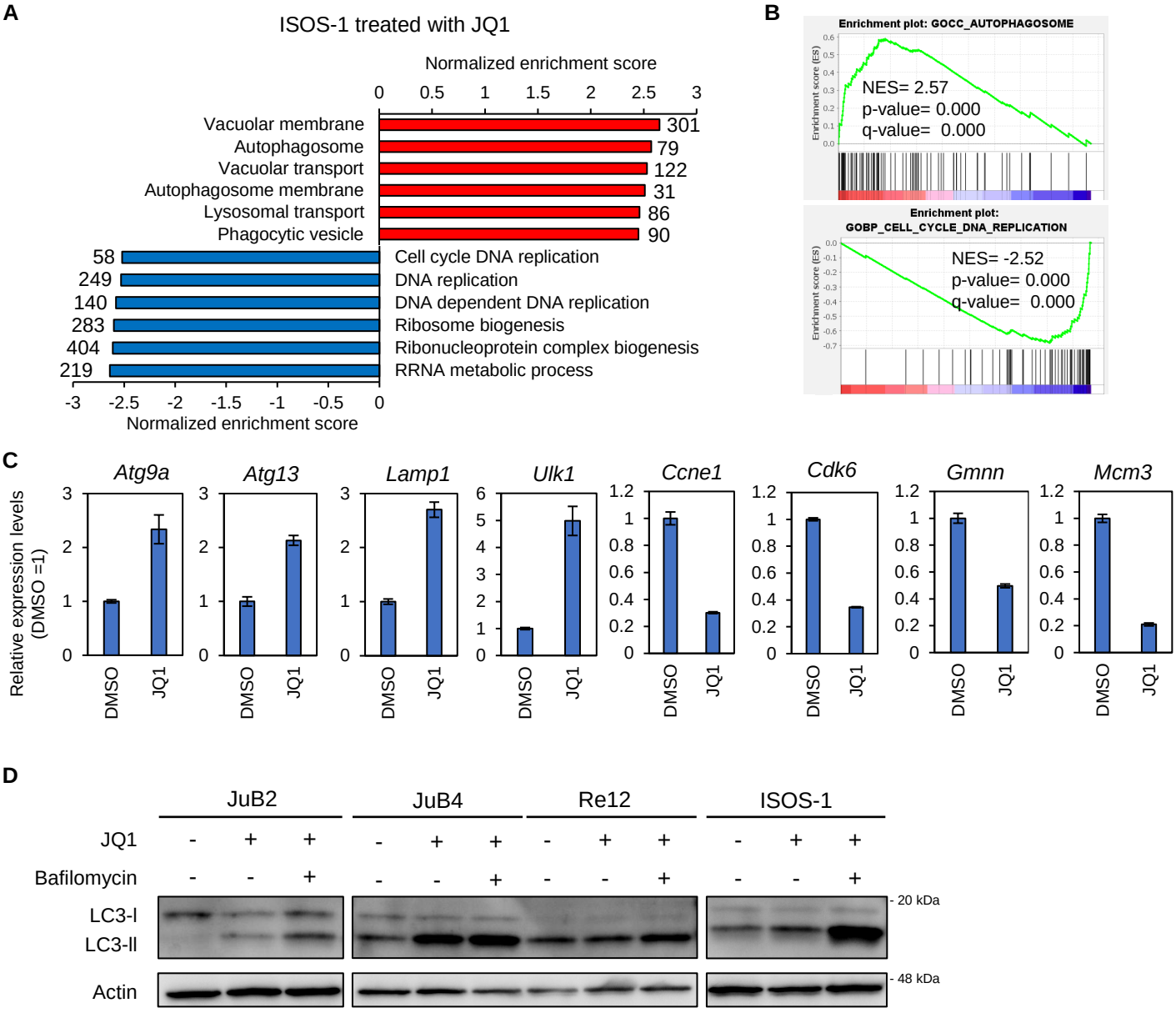
A
ISOS-1 treated with JQ1
Normalized enrichment score
0 0.5 1 1.5 2 2.5 3
Vacuolar membrane 301
Autophagosome 79
Vacuolar transport 122
Autophagosome membrane 31
Lysosomal transport 86
Phagocytic vesicle 90
58 Cell cycle DNA replication
249 DNA replication
140 DNA dependent DNA replication
283 Ribosome biogenesis
404 Ribonucleoprotein complex biogenesis
219 RRNA metabolic process
-3 -2.5 -2 -1.5 -1 -0.5 0
Normalized enrichment score
B
Enrichment plot: GOCC_AUTOPHAGOSOME
Enrichment score (ES)
NES= 2.57
p-value= 0.000
q-value= 0.000
Enrichment plot:
GOBP_CELL_CYCLE_DNA_REPLICATION
Enrichment score (ES)
NES= -2.52
p-value= 0.000
q-value= 0.000
C
Relative expression levels (DMSO =1)
Atg9a
Atg13
Lamp1
Ulk1
Ccne1
Cdk6
Gmnn
Mcm3
DMSO
JQ1
D
JuB2
JuB4
Re12
ISOS-1
JQ1
Bafilomycin
LC3-I
LC3-II
Actin
20 kDa
48 kDa

Fig.4

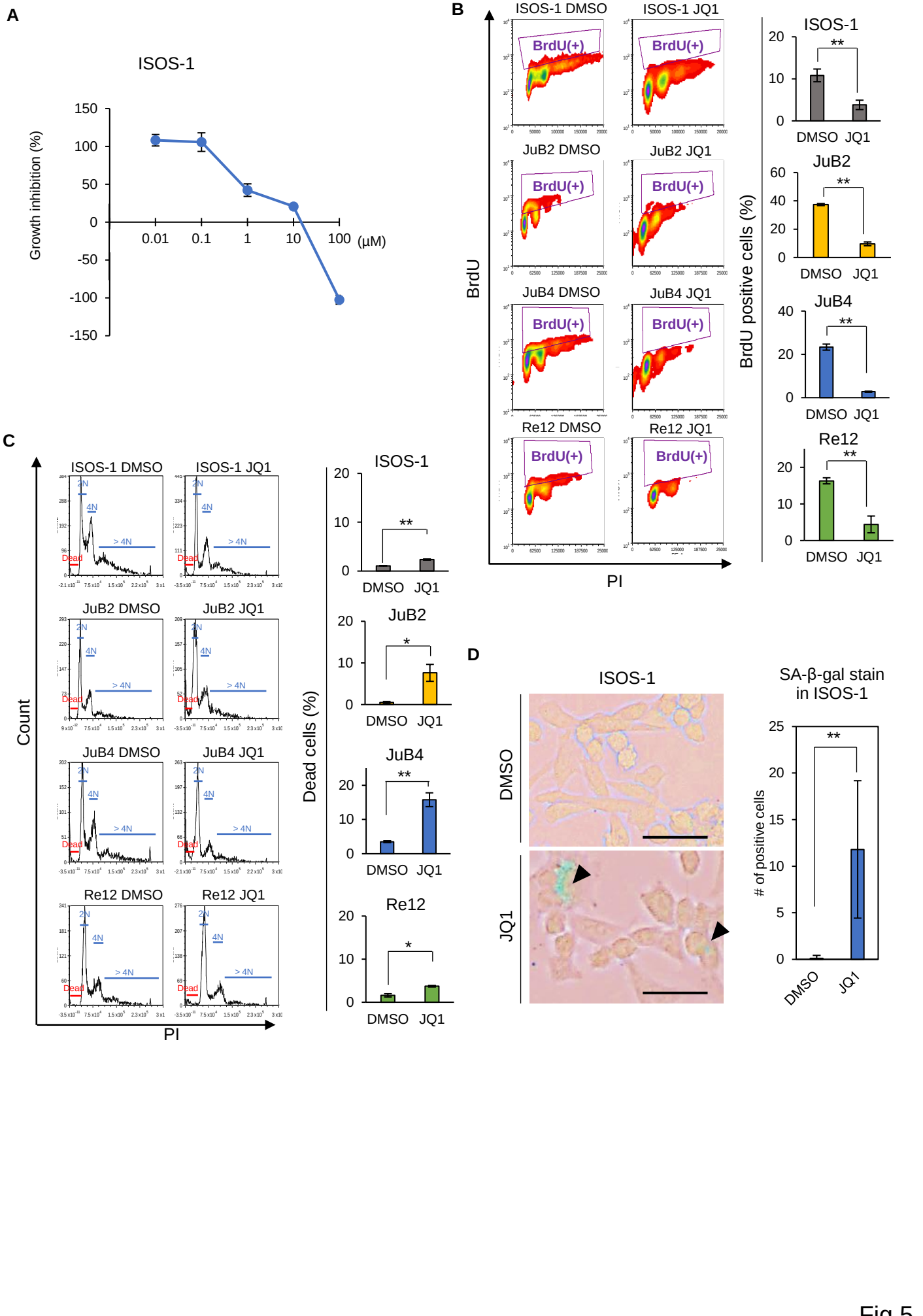
A
ISOS-1
Growth inhibition (%)
150
100
50
0
-50
-100
-150
0.01
0.1
1
10
100
(μM)
B
ISOS-1 DMSO
ISOS-1 JQ1
JuB2 DMSO
JuB2 JQ1
JuB4 DMSO
JuB4 JQ1
Re12 DMSO
Re12 JQ1
BrdU(+)
BrdU
PI
BrdU positive cells (%)
ISOS-1
JuB2
JuB4
Re12
DMSO
JQ1
**
C
Count
PI
2N
4N
> 4N
Dead
Dead cells (%)
ISOS-1
JuB2
JuB4
Re12
*
**
D
ISOS-1
DMSO
JQ1
SA-β-gal stain in ISOS-1
# of positive cells

Fig.5

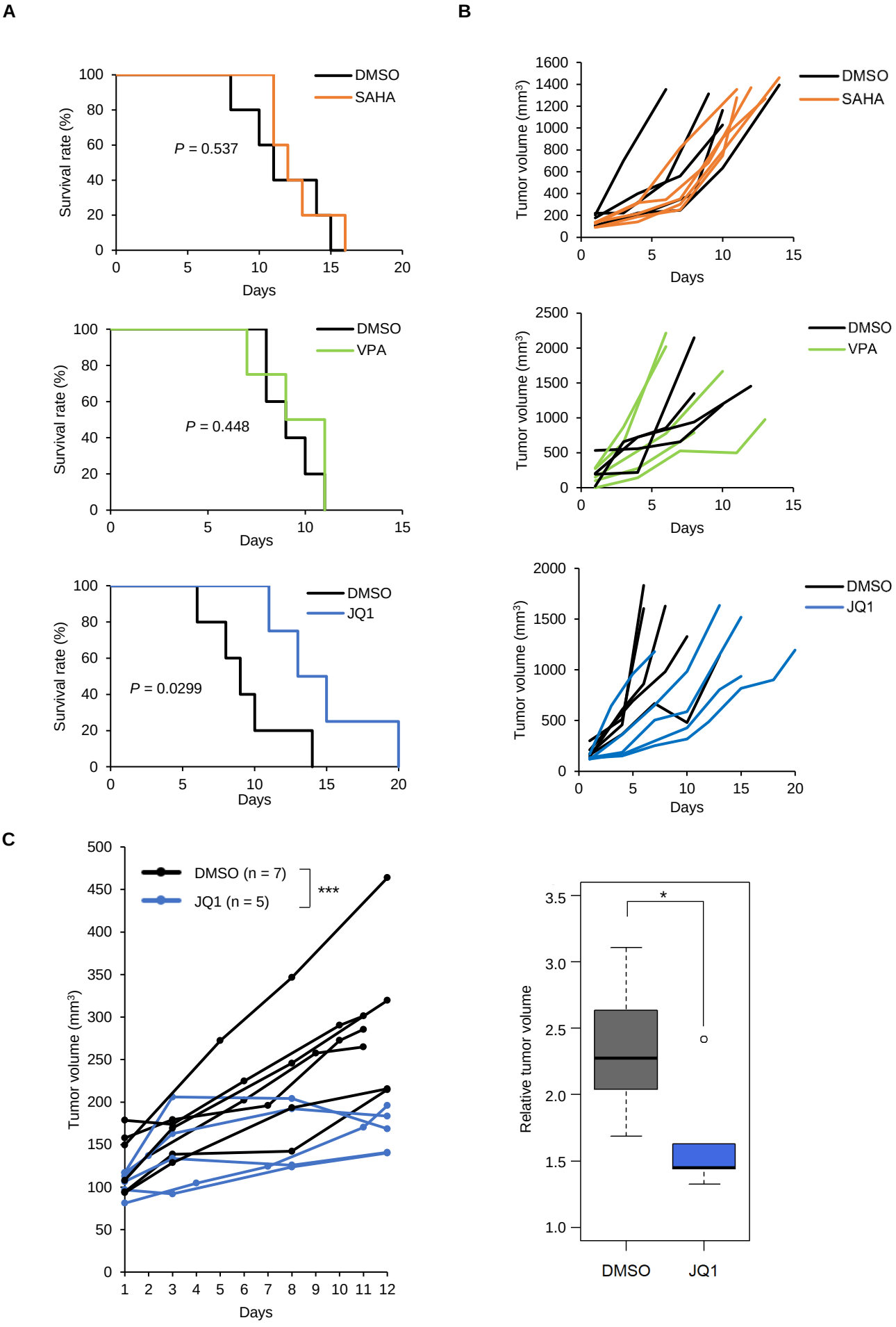
A
B
C
Survival rate (%)
Days
DMSO
SAHA
P = 0.537
VPA
P = 0.448
JQ1
P = 0.0299
Tumor volume (mm³)
DMSO (n = 7)
JQ1 (n = 5)
***
Relative tumor volume
*

Fig.6